Desalination and Water Treatment
www.deswater.com

doi: 10.5004/dwt.2022.28406

256 (2022) 163–175
April

Removal of oil spills by novel developed amphiphilic chitosan-*g*-citronellal Schiff base polymer: kinetic, isotherm, and thermodynamic studies

Basant Y. Eweida[a], Tamer M. Tamer[b], Ahmed M. Omer[b], Hesham M.A. Soliman[c], Ahmed A. Zaatot[d], Mohamed S. Mohy-Eldin[b,*]

[a]*Modeling and Simulation Department, Advanced Technology and New Materials Research Institute, City of Scientific Research and Technological Applications (SRTA-City), New Borg El-Arab City, Alexandria 21934, Egypt, email: bewida@srtacity.sci.eg*
[b]*Polymer Materials Research Department, Advanced Technology and New Materials Research Institute (ATNMRI), City of Scientific Research and Technological Applications (SRTA-City), New Borg El-Arab City, Alexandria 21934, Egypt, Tel. +20 34593414; email: mmohyeldin@srtacity.sci.eg (M.S. Mohy-Eldin) ORCID: 0000-0003-2228-211X, emails: tmahmoud@srtacity.sci.eg (T.M. Tamer), amomar@srtacity.sci.eg (A.M. Omer)*
[c]*Nanotechnology and New Composite Materials Department Advanced Technology and New Materials Research Institute (ATNMRI), City of Scientific Research and Technological Applications (SRTA-City), New Borg El-Arab City, Alexandria, 21934, Egypt, email: h.soliman@srtacity.sci.eg*
[d]*Chemical Engineering Department, Faculty of Engineering, Alexandria University, Egypt, email: ahmed.zaatoot@alexu.edu.eg*

Received 12 October 2021; Accepted 14 March 2022

ABSTRACT

A novel chitosan-*g*-citronellal Schiff base oil adsorbent material based on chitosan was developed and evaluated successfully to remove oil spills. Chitosan was first prepared from wastes of marine shrimp shells, and then chitosan-*g*-citronellal Schiff base was synthesized. The kinetic studies of the heavy oil spills removal by adsorption process were carried out using different models, namely, pseudo-first-order, pseudo-second-order, and the oil diffusion control process studied by both intraparticle diffusion models. The results indicate that the pseudo-second-order equation fitted the experimental data better than the pseudo-first-order equation for its higher R^2 (all R^2 values are closed to 1). Langmuir, Freundlich, and Harkins–Jura adsorption isotherm models investigated the isotherm of the removal process under equilibrium conditions. The correlation coefficient R^2 values indicate a good mathematical fit for the adsorption process of heavy crude oil to both Langmuir and Freundlich models. The Langmuir monolayer oil adsorption capacity of chitosan-*g*-citronellal Schiff base (22 g g^{-1}) was found about 245% of the chitosan (9 g g^{-1}) within the studied conditions. Furthermore, the thermodynamic of the process has also been depicted. The thermodynamic studies revealed that sorption was spontaneous and endothermic. Furthermore, the recyclability of the developed chitosan-*g*-citronellal Schiff base has been proved while kept 77% of its oil adsorption capacity after seven cycles compared with 50% of the chitosan counterpart. The structure of the chitosan and chitosan-*g*-citronellal Schiff base adsorbents were verified using nuclear magnetic resonance spectroscopy, Fourier-transform infrared spectroscopy and thermal gravimetric analysis. Moreover, the morphological changes followed using scanning electron microscopy. The Brunauer–Emmett–Teller analysis of the developed chitosan-*g*-citronellal Schiff base exhibited a higher surface area compared to neat chitosan.

Keywords: Chitosan-*g*-citronellal; Amphiphilic; Schiff base; Oil spill removal; Kinetics; Isothermal; Thermodynamic studies

* Corresponding author.

1. Introduction

Energy and raw materials are the essential foundations for any development. Based on those principles, crude petroleum oil gained importance in providing energy and synthesizing synthetic polymers and chemicals worldwide [1,2]. The processes and activities related to crude petroleum oil and its derivatives may result in oil spillage [3], which has powerful drawbacks as direct or indirect effects on human life and the environment [4]. Elimination of those drawbacks takes a long time and too much effort [4]. Among different techniques and methods used in oils spills removal, the adsorption process comes in the front. The oil uptake by the adsorbents goes through multistep according to the interaction that occurs at the surface, internal structure, and finally pores of the adsorbent, and can be concluded in the following sequences; diffusion, entrapment, and finally oil droplets agglomeration [5]. Accordingly, the oil separated from the liquid water phase, then handled [2,6]. The oils adsorbents can be classified based on their origin and must have two essential characters; high capacity to sorb oil and repel water [7,8]. The natural origin oil adsorbents have been obtained by chemical treatment of many natural products [9]. Adebajo et al. [10] review the synthesis and the absorbing properties of the wide variety of porous sorbent materials that have been studied for application in the removal of organics, particularly in the area of oil spills clean up. The discussion is mainly focused on hydrophobic silica aerogels, zeolites, organoclays and natural sorbents, many of which have been demonstrated to exhibit (or show potential to exhibit) excellent oil absorption properties. The areas for further development of some of these materials are identified. Alaa El-Din et al. [11] reviewed the oil sorption capacity of crude and gas oils, using banana peel as a substitution material from local fruit wastes. The research detected that the capacity of this sorbent to clean up crude oil from produced water toward different factors is associated with surface characteristics, oil type, oil film thickness, sorption time, temperature, in addition to the salinity of crude oil. Wolok et al. [12] discussed the urgent requirement of advanced eco-friendly tools to eliminate spilt oil and summarized the overall perspective on the potential of different biomaterials to remove accidentally spilt oils.

Hoang et al. [13] recently reviewed the advanced super-hydrophobic polymer-based porous absorbents to treat oil-polluted water. In general, this paper has provided an overview and a comprehensive assessment of the use of advanced polymer-based porous materials to treat oil-polluted water. Two types of polymer-based porous absorbents, modified surface and structure, were introduced for the treatment strategy of the oil-polluted water. In addition, the absorption mechanism and factors affecting the adsorption capacity for oils and organic solvents were thoroughly analyzed. More importantly, characteristics of polymer-based porous materials were discussed in detail based on microstructure analysis, absorption efficiency, and reusability. Chitosan is among the natural materials used to develop oil adsorbents [1,2] based on their functional groups' modifications [9]. Modification of the chitosan' amine groups via reaction Modifying ketones to have Schiff bases is well known and heavily investigated [14,15].

In our previous study [16], novel chitosan-grafted-citronellal Schiff base (Ch-*g*-Cit) amphiphilic polymer was developed for the adsorptive removal of oil spills. The amphiphilic character of the Ch-*g*-Cit Schiff base was controlled through variation of the grafting percentage (*G* %) of citronellal from 11% to 61%. The results substantiate that the amphiphilic Ch-*g*-Cit Schiff base could be efficiently applied as a low-cost oil adsorbent to remove crude oil spills from seawater surfaces.

Our previous research project was to develop chitosan derivatives for oil spills applications carried out in two steps. As first step, chitosan modified to have aminated chitosan and nonanyl chitosan Schiff base [17]. The second-step was the grafting of chitosan [18], aminated chitosan [19], and nonanyl chitosan [20] with hydrophobic–oleophilic polymers (polybutylacrylate). Furthermore, and for a better understanding of the oil spills removal process, the kinetic, isotherm, and thermodynamic parameters have been studied for the developed chitosan derivatives [21], chitosan grafted poly(butyl acrylate) [22], nonanyl chitosan-grafted-poly(butyl acrylate) [20], and aminated chitosan-*g*-poly(butyl acrylate) copolymer [23].

This study focused on the kinetic, isothermal, and thermodynamic studies for the oil spills removal by the novel amphiphilic chitosan-*g*-citronellal Schiff base polymer developed in our previous study [16] and compared with native chitosan. In addition, the recyclability of the developed chitosan-*g*-citronellal Schiff base compared with the chitosan counterpart has been studied.

2. Materials and methods

2.1. Materials

Sodium hydroxide pellets were obtained from EL. Pharanae Co., (assay 99%, M_{wt} = 40 g mol^{-1}). Acetic acid (purity 99.8%, M_{wt} = 60.05 g mol^{-1}), glutaraldehyde (GA; 99%), citronellal (purity ≥ 95%, M_{wt} = 154.25 g mol^{-1}). Ethanol (purity 99%), hydrochloric acid (assay 37%), ethyl alcohol absolute were brought from El-Nasr Company (Alexandria). Shrimp skeletons were provided from a commercial resource in Alexandria (Egypt). Sodium chloride and sulfuric acid (purity 95%–97%) was purchased from El-Gomhouria Co., (Egypt). Egyptian heavy crude oil sample was supplied from Belayem Petroleum Company, Egypt.

2.2. Methods

2.2.1. Preparation of chitosan

Crushed shells are first treated with 10% hydrochloric acid to remove calcium salts, followed by protein and lipids removal with 10% sodium hydroxide to obtain chitin, then dried at 50°C overnight. Chitin thus obtained was hydrolyzed using 50% sodium hydroxide at a high temperature (100°C–150°C) to provide chitosan [24,25]. Finally, chitosan obtained dried at 50°C overnight [26,27]. The chitosan sample was dissolved in 2% acetic acid and left overnight. The solution was then filtrated through cheesecloth to remove contaminants and un-dissolved particles, then 100 μL of GA and stirred for 1 h at 80°C. The obtained GA-chitosan was then precipitated with 5% sodium hydroxide,

collected and washed with distilled water to remove the excess of alkali and coded as (CH-CIT0) [24].

2.2.2. Preparation of chitosan-g-citronellal Schiff base

The chitosan-*g*-citronellal Schiff base adsorbent was prepared according to a previously published method [16] using solutions of chitosan-*g*-citronellal with two different molar ratios 1:0.85 and 1:4.25, given 33.25% *G* and 56.25% *G*, and coded as CH-CIT2, and CH-CIT5 adsorbents samples.

2.2.3. Physicochemical characterization

2.2.3.1. Fourier-transform infrared spectroscopy

The chitosan and chitosan-*g*-citronellal Schiff base structures were investigated by Fourier-transform infrared spectroscopic analyses using Fourier-transform infrared spectrophotometer (Shimadzu FTIR-8400S, Japan). Samples (2–10 mg) were mixed thoroughly with KBr, and the absorbance of samples was scanned from 500–4,000 cm^{-1}.

2.2.3.2. Thermal gravimetric analysis

Analysis by thermal gravimetric analysis (TGA) of samples was carried out using a thermogravimetric analyzer (Shimadzu TGA –50, Japan) under nitrogen, at a gas flow rate of 20 mL min^{-1}, to evidence changes in structure as a result of the modification. In addition, samples were measured their weight loss starting from room temperature to 800°C at a heating rate of 10°C/min.

2.2.3.3. Scanning electron microscopic analysis

Samples were fixed on aluminium stubs and vacuum coated with gold before being examined by scanning electron microscopy (SEM). Morphological changes of the sample's surface were followed using a secondary electron detector of SEM (Joel Jsm 6360LA, Japan). Magnifications factor 1000X was used under 20 KeV.

2.2.3.4. Nuclear magnetic resonance spectrometer

Nuclear magnetic resonance spectrometer (^{1}H NMR; JEOL 500 MH, Japan) was used to determine the DD and verify chitosan and chitosan-*g*-citronellal samples structures, respectively.

2.3. Brunauer–Emmett–Teller analysis

Besides, the specific surface area and pores size of the developed chitosan and chitosan-*g*-citronellal adsorbents was measured by the Brunauer–Emmett–Teller method (BET-Beckman coulter SA3100).

2.3.1. Determination of ion-exchange capacity

A known weight of chitosan or chitosan derivatives were added to a known volume of 0.1 M H_2SO_4 solution, and the mixture was kept aside for two h. Then, the mixture was filtered, and an aliquot was titrated against a standard sodium hydroxide solution. Similarly, control titration without the addition of chitosan was also run. From the difference in the volume of NaOH required for neutralization, the ionic capacity of chitosan samples was calculated using the following equation:

$$\text{Ion exchange capacity} = \frac{\left(V_2 - V_1\right)A}{W} \tag{1}$$

where V_2 and V_1 are the volumes of NaOH required for complete neutralization of H_2SO_4 in the absence and presence of chitosan, respectively, A is the normality of NaOH and W is the weight of the sample taken for analysis.

2.3.2. Water uptake

Water uptake estimation was performed by placing a weighed sample in 10 ml water. After 6 h the sample was then filtered off, carefully bolted with a filter paper and weighed. The water uptake was calculated by applying the following equation:

$$\text{Water uptake} = \left[\frac{\left(M - M_o\right)}{M_o}\right] \tag{2}$$

where M is the weight of the swelled sample at time t, and M_o is the weight of the dry sample [24,26].

2.3.3. Oil uptake

Oil uptake was calculated by soaking a known weight of the samples (0.05 g) in 10 mL of oil (mineral oil, diesel oil, kerosene oil) and then placed in a closed glass container for different time intervals carefully bolted with a filter paper and weighed immediately in a closing balance. The following equation can express oil uptake:

$$\text{Oil uptake} = \left[\frac{\left(W_t - W_o\right)}{W_t}\right] \tag{3}$$

where W_t is the weight of the soaked sample in the oil for a certain time, and W_o is the sample initial dry weight [24,26]. For regeneration study, the adsorbed oil was extracted through using 10 mL of *n*-hexane, as the solvent, for 7 successive times with shaking in water bath thermo-stated at 35°C for 30 min followed by washing with 10 mL of ethanol for 5 successive times then dried at 65°C overnight before reused in the following adsorption experiments.

3. Results and discussion

3.1. Materials characterization

Table 1 shows the changes in the water uptake and the ion-exchange capacity of the native chitosan due to the chitosan-*g*-citronellal Schiff base formation. From the table, increasing the citronellal ratio to chitosan increases the formation of Schiff base between its aldehyde groups and

Table 1
Water uptake and ion-exchange capacity of chitosan and chitosan-*g*-citronellal derivatives

Sample code	Water uptake (g g^{-1})	Ion-exchange capacity (meq g^{-1})
CH-CIT0	1.9	9.95
CH-CIT2	1.05	5.81
CH-CIT5	0.15	2.92

amino groups of chitosan. This consumption of the amino groups leads consequently to a decrease of its ion-exchange capacity from 9.95 of chitosan to 5.81 and 2.92 meq g^{-1} of CH-CIT2 and CH-CIT5. The same trend was observed when chitosan interacted with aldehydes and ketones [24]. Water uptake (WU) of the chitosan-*g*-citronellal Schiff base displays a remarkable decrease of water uptake of chitosan [28] where the water uptake decreased from 1.9 g g^{-1}, for chitosan, to 1.05 and 0.15 g g^{-1} of CH-CIT2 and CH-CIT5. That was a direct result of changing the hydrophilic nature of chitosan to hydrophobic one by grafting with hydrocarbon chains of citronellal [24].

3.2. Fourier-transform infrared spectroscopy analysis

Fig. 1A represents Fourier-transform infrared spectroscopy (FTIR) of chitosan and chitosan-*g*-citronellal Schiff base. Chitosan demonstrates the typical bands of chitosan function groups; broadband between 3,425 cm^{-1} matching the stretching vibration of NH_2 and OH groups distributed along the polymer backbone. The weak absorption peak at 2,895 cm^{-1} (C–H stretch) for methyl and methylene groups, the characteristic peak of chitosan at 1,624 cm^{-1} assigned to the C=O stretching [29]. The band at 1,070 cm^{-1} ascribed to the stretching of the C–O–C bridge [30].

Chitosan-*g*-citronellal Schiff base shows a significant change in FTIR spectra. The significant differences are in the broad peaks at 3,425 cm^{-1} for chitosan and 3,419 cm^{-1} for chitosan-*g*-citronellal Schiff base that can be attributed to the consumption of chitosan amine groups in the Schiff base formation process. Also, absorption bands at 2,921 cm^{-1} for chitosan-*g*-citronellal Schiff base absorption bands due to –CH stretching.

As the molar ratio between chitosan and citronellal was increased, the spectrum displays firm absorption peaks at 1,606 cm^{-1} corresponding to the C=N stretching, which formed between the aldehyde group and chitosan. At the same time, the peak at 1,624 cm^{-1} was weakened.

3.3. NMR analysis

^{1}H NMR spectrum was employed to investigate the chemical structure of the new synthesized chitosan-*g*-citronellal Schiff base and estimate the degrees of deacetylation and substitution. All NMR spectra were accumulated under identical conditions using power gated Waltz decoupling with 25° measurement pulse and 1 s pre-pulse delay. Fig. 1B shows the characteristic chemical shift of proton in the amino glucose ring of chitosan as δ 2.5 ppm from the three methyl H atoms (GlcNAc), δ 2.88 ppm from H2 (GlcN). Several overlapping signals from δ 3.4 to 3.60 ppm are detected, which refer to H3–H6 connected to the non-anomeric C3–C6 carbons in the glucopyranose ring, and ca. δ 5.1 ppm from anomeric proton (H1) [31–33]. Moreover, the deacetylation degree of chitosan was calculated and recorded a maximum value of 95.4% [34]. Besides, the chitosan-*g*-citronellal (CH-Cit) Schiff base (Fig. 1C) demonstrated a complicated chart as its new signals overlapped with the neat chitosan polymer. The characteristic peak at δ 7.9–8 ppm refers to the immune proton (H10). The new signal at 0.9–1 ppm could be attributed to the protons of methyl groups (H13). Furthermore, the observed new overlapped signals at δ 1.18–1.43 ppm refer to H11 and H14, while the multi signals at δ 1.7–1.8 could be related to methylene protons H12, H15.H17 and H18. The proton signal for unsaturated carbon (H16) was overlapped with H1 and H7 in chitosan at δ 5.1–5.2 ppm. The degree of substitution was determined and recorded 17.7% of citronellal substitution.

3.4. Thermal gravimetric analysis

Fig. 1D represents the thermal gravimetric analysis of CH-CIT0, CH-CIT2 and CH-CIT5. Chitosan demonstrates three weight loss steps. The first weight loss that starts from ambient temperature to about 150°C was related to elevated moisture molecules entrapped between the polymer chains. The presence of hydrophilic groups (hydroxyl and amine groups) along the polymer backbone can explain the polymer's ability to trap moisture from the surrounding atmosphere. The subsequent second degradation that was recognized from 210°C to 320°C resulted from the oxidative decomposition of the chitosan backbone. In this stage, the first depression was produced from the destruction of amine groups to form cross-linked fragments [35]. The third depuration that results from the decomposition, which appears at high temperature, may produce from the thermal degradation of a new cross-linked material formed by thermal cross-linking reactions occurring in the first stage of the degradation [36].

There is a noticeable difference in thermal stability between chitosan and chitosan-*g*-citronellal Schiff base due to the temperature required to lose their half weights (T_{50}%), ranging from 315°C to 360°C as represented in Table 2. First, the T_{50} of the CH-CIT2 was improved from ≈343°C of chitosan to 360°C. However, further Schiff base formation (CH-CIT5) shows a significant lower of the T_{50}, which reaches ≈316°C. The significantly less stability of Schiff base derivatives is confirmed with published results in the literature [27].

3.5. Scanning electron microscopic analysis

The surface morphological analysis of chitosan and chitosan-*g*-citronellal Schiff base samples was studied using a SEM (Fig. 1E). The SEM graphs show a remarkable increase of surface roughness as increase the modification [24]. Where CH-CIT2 is the appearance of noodles and rodless structure in addition to microparticles structure (Fig. 1F), the existences of different shapes may attribute to the change of hydrophilic–hydrophobic balance of the newly

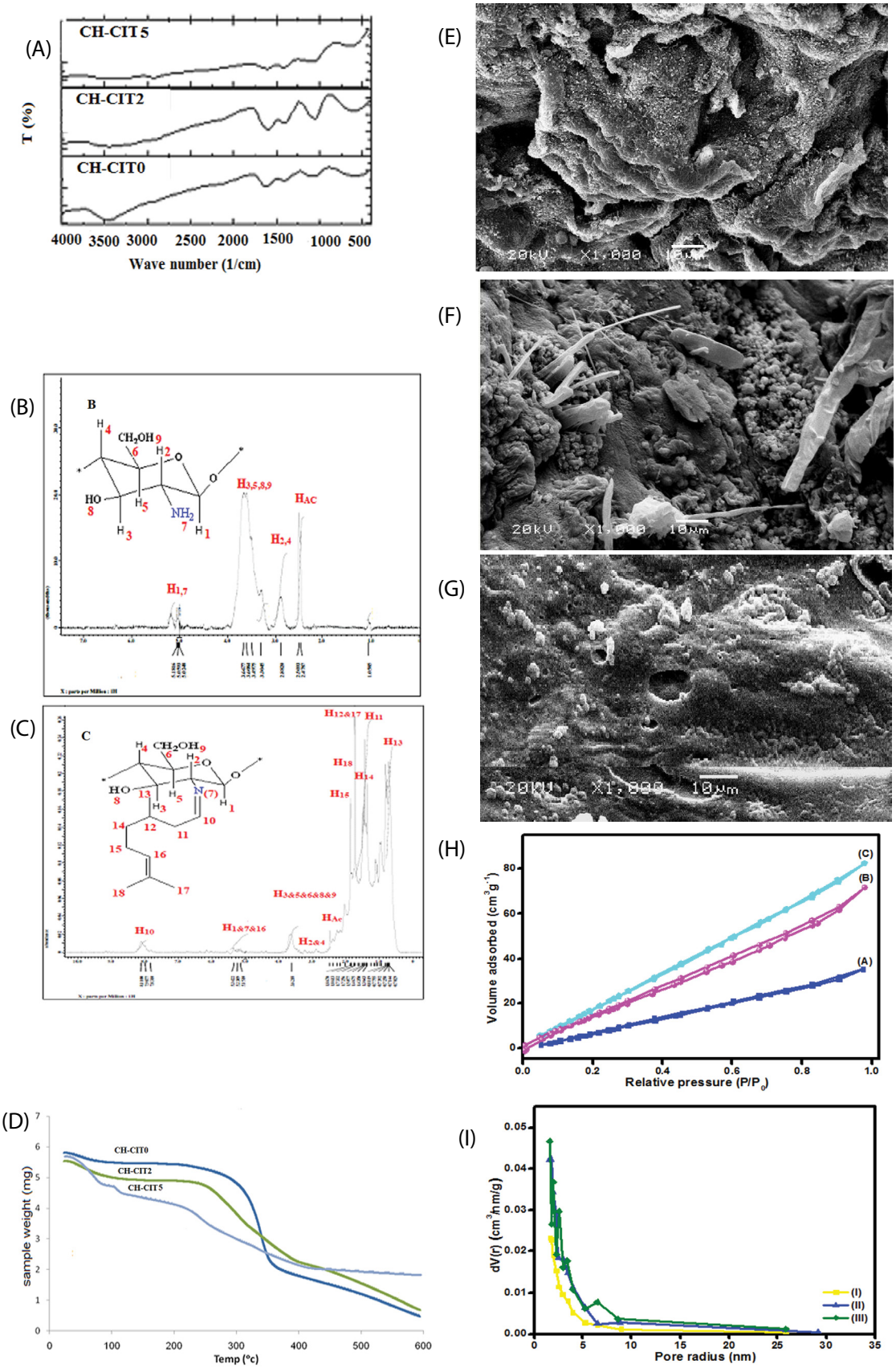

Fig. 1. (A) FTIR spectra of CH-CIT0, CH-CIT2, and CH-CIT5. ^{1}H NMR of (B) chitosan and (C) chitosan-*g*-citronellal Schiff base. (D) TGA of CH-CIT0, CH-CIT2, and CH-CIT5. SEM of (E) CH-CIT0, (F) CH-CIT2, and (G) CH-CIT5. (H) S_{BET} of (A) CH-CIT0, (B) CH-CIT2, and (C) CH-CIT5. (I) Pore radius of (I) CH-CIT0, (II) CH-CIT2, and (III) CH-CIT5.

Table 2
Thermal gravimetric parameters of CH-CIT0, CH-CIT2 and CH-CIT5

Sample code	Weight loss (%) ambient-150°C	T_{50} (°C)
CH-CIT0	6.02	342.81
CH-CIT2	11.19	360.27
CH-CIT5	22.73	315.92

formed Schiff base. Moreover, the reduction of the water content and the heterogeneity of the reaction of aldehyde and the amino groups of the chitosan backbone could explain the obtained morphology characters. That will stimulate a change in the internal forces between polymer chains and may also induce changes of solid-state crystalline [6]. Further substitution of amino groups and formation of Schiff base in case of CH-CIT5 leads to turn the nature of the formed Schiff base to a hydrophobic one where less water uptake detected as seen in Table 1. The morphology changes where the noodles and rodless structure in addition to microparticles structure noticed in CH-CIT2 disappeared, and the surface morphology turned to be minor roughness with a coating layer appeared (Fig. 1G).

3.6. BET analysis

BET analysis was performed to scrutinize the influence of different concentrations of citronellal on the specific surface area (S_{BET}) and the pore diameter of chitosan and its Schiff base derivatives. The results depicted in Fig. 1H signified that that chitosan and chitosan-*g*-citronellal Schiff base derivative display type II. Furthermore, a noticeable improvement in the S_{BET} of the chitosan Schiff bases compared to the neat chitosan since the S_{BET} of CH-CIT0, CH-CIT2, and CH-CIT5 Schiff bases were 57.78, 74.84 and 112.09 $m^2\ g^{-1}$, respectively. Furthermore, The Barrett–Joyner–Halenda pore size distributions (Fig. 1I) revealed the mesopores structures of native chitosan and chitosan-*g*-citronellal Schiff bases. The results referred that the pore radius of CH-CIT0, CH-CIT2, and CH-CIT5 Schiff bases were 2.2, 2.95 and 3.50 nm, respectively.

3.7. Oil spills adsorption process

From the previous characterization, it can be concluded that the ion-exchange capacity of the CH-CIT5 is the lowest, 2.92 meq g^{-1}, compared with chitosan, 9.95 meq g^{-1}, and CH-CIT2, 5.81 meq g^{-1} and the same finding was observed with the water uptake (WU) of the CH-CIT5, 0.15 g g^{-1}, compared with chitosan, 1.9 g g^{-1}, and CH-CIT2, 1.05 g g^{-1}. Moreover, the S_{BET} of the CH-CIT5 was found the highest, 112.09 $m^2\ g^{-1}$, compared with chitosan, 57.78 $m^2\ g^{-1}$, and CH-CIT2, 74.84 $m^2\ g^{-1}$. Furthermore, the pore size distributions reinforced the hydrophobicity, low ion-exchange capacity and high surface area advantages. The results referred that the pore radius of CH-CIT0, CH-CIT2, and CH-CIT5 Schiff bases were 2.2, 2.95 and 3.50 nm, respectively. According to these privileges of CH-CIT5, Schiff base has been selected to study the kinetic, isothermal, and thermodynamic studies for the oil spills removal compared to native chitosan.

3.7.1. Effect of the adsorption' time and adsorption kinetics

The adsorption time has a positive linear impact on the adsorption capacity of both chitosan and chitosan-*g*-citronellal matrices until 90 min (Fig. 2A). Beyond 90 min, the adsorption capacity increment rate started to be lower and levelled off after 120 min. Thus, the adsorption capacity of the chitosan-*g*-citronellal towards oil was significantly improved compared to chitosan. The adsorption capacity levelling off after 120 min of adsorption time referred to two opposite reasons [37]. The first concerns the adsorbent, where all adsorption sites over the adsorbent surface were consumed, and the interior pores were filled. The second reason concerns the available oil amounts. The first reason for the chitosan adsorbent is that only 40% of the oil was removed after 120 min. On the other side, the second reason is the determining factor for the chitosan-*g*-citronellal, where 98% of the amounts of the oil were removed after 120 min. This behaviour is expected due to the hydrophobic nature of the chitosan-*g*-citronellal sorbent material, which enables it to attach oil molecules easily on the adsorbent surface and inside its porous structures. Therefore, the number of the attached molecules increased with increasing the contact time between oil and Schiff base which significantly enhances the adsorption capacity.

The knowledge of adsorption kinetics is essential information for designing batch adsorption systems. The pseudo-first-order and pseudo-second-order kinetic models and intraparticle diffusion models were examined of chitosan and chitosan-*g*-citronellal Schiff base for heavy crude oil [38–42]. The kinetic models are represented by the following linear form equations:

$$\ln\left(q_e - q_t\right) = \ln q_e - k_1 t \tag{4}$$

$$\frac{t}{q_t} = \frac{1}{k_2 q_e^2} + \frac{t}{q_e} \tag{5}$$

where q_e is the amount of adsorption at equilibrium, g g^{-1}; q_t is the amount of adsorption at time t, g g^{-1}; k_1 is the first-order rate constant, min^{-1}; k_2 is the second-order rate constants, min^{-1}.

Constants of pseudo-first-order and pseudo-second-order were determined experimentally by plotting $\log(q_e - q_t)$ vs. t for pseudo-first-order and plotting a t/q_t against t, from Fig. 2B and 2C.

The conformity between experimental data and the model predicted values was expressed by correlation coefficient (R^2). Comparing Fig. 2B with Fig. 2C, we found that the pseudo-second-order equation fitted the experimental data better than the pseudo-first-order equation for its higher R^2 (all R^2 values are closed to 1) [38].

The amount of adsorption equilibrium q_e, the rate constants of the equation, k_1 and k_2, the calculated amount of

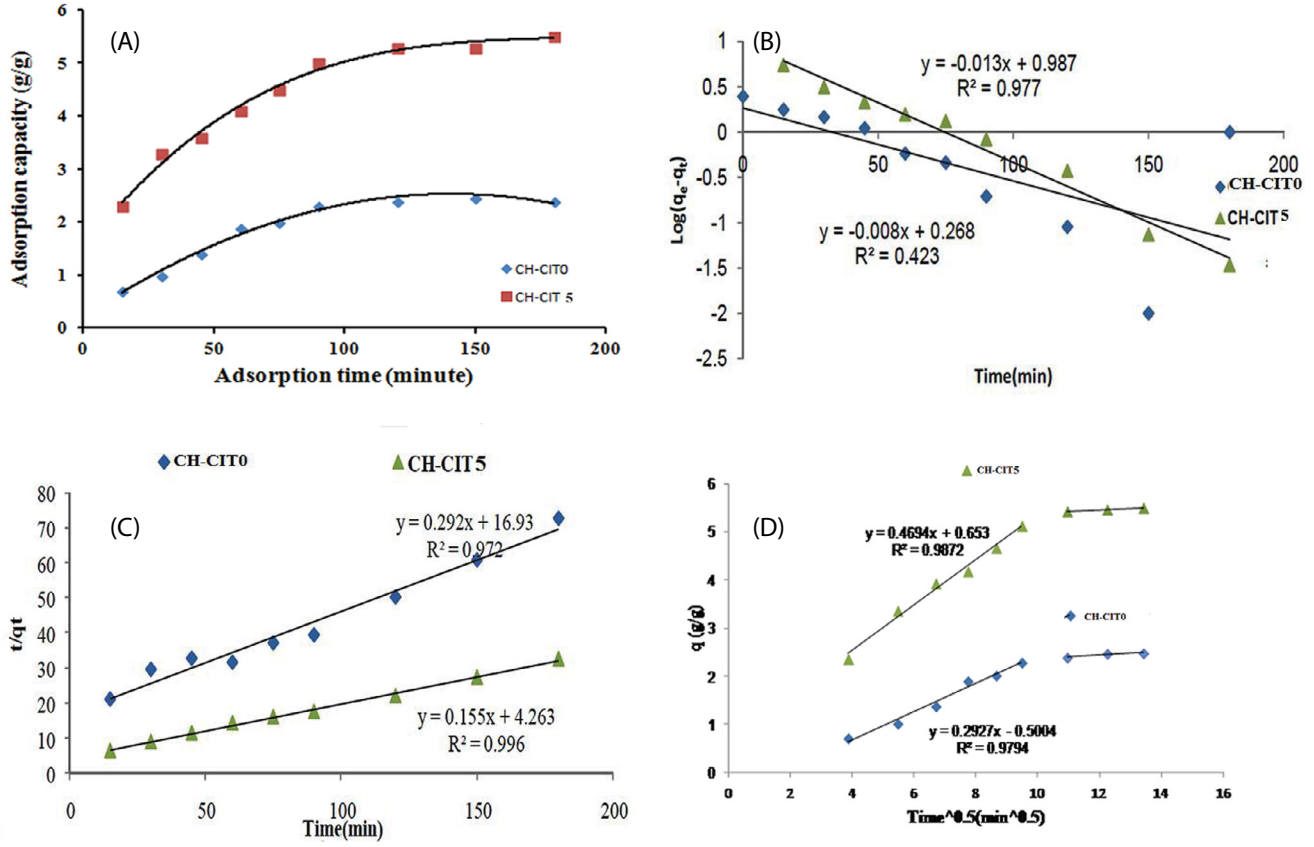

Fig. 2. (A) Effect of the contact time on adsorption capacity of the chitosan and the chitosan-*g*-citronellal Schiff base adsorbents. Fitting of heavy crude oil adsorption process with (B) pseudo-first-order, (C) pseudo-second-order, and (D) intraparticle diffusion model.

Table 3
Kinetic parameters for heavy crude oil adsorption with chitosan and chitosan-*g*-citronellal Schiff base

Samples	Pseudo-first-order				Pseudo-second-order				Intraparticle diffusion		
	$q_{e(exp)}$ (g g^{-1})	$q_{e(cal)}$ (g g^{-1})	k_1 (g g^{-1} min^{-1})	R^2	$q_{e(cal)}$ (g g^{-1})	k_2 (g g^{-1} min^{-1})	h (mol g^{-1} min^{-1})	R^2	K_P (g g^{-1} min$^{-1/2}$)	C (g g^{-1})	R^2
Chitosan	2.474	1.85	0.0184	0.423	3.42	0.0063	0.059	0.972	0.292	–0.5	0.979
Chitosan-*g*-citronellal Schiff base	5.501	9.71	0.0299	0.977	6.45	0.0055	0.235	0.996	0.469	0.653	0.987

adsorption equilibrium, $q_{e(cal)}$ and the coefficient of determination, R^2, for heavy oil are shown in Table 3. From the table, it can be seen that oil adsorption rate constant k_2 in the case of chitosan greater than chitosan-*g*-citronellal Schiff base, which indicates faster rate diffusion of heavy oils in case of adsorption by chitosan, but adsorption capacity (q_e) of chitosan-*g*-citronellal Schiff is higher than of chitosan in cases of heavy crude oils [38]. As well, the initial sorption rate (h; (mol g^{-1} min^{-1})) was faster in case of the chitosan-*g*-citronellal Schiff base than in the chitosan adsorbent. The obtained kinetic results are following our previous study of oil spills adsorption using developed nonanyl chitosan Schiff base [21].

Prediction of the oil diffusion mechanism during the sorption process performed through using intraparticle diffusion model according to the following equation;

$$q_t = k_p t^{1/2} + C \tag{6}$$

where k_p is the intraparticle diffusion constant (g g^{-1} min$^{-1/2}$).

Fig. 2D shows the plot of oil sorption capacity (g g^{-1}), q_t vs. $t^{1/2}$ for heavy crude oil adsorption. The intraparticle diffusion plot confirms that the adsorption occurs in 2 steps. The first, sharper region, fastest step, the plot is linear due to mass transfer which is attributed to the diffusion of oil transported from the bulk solution to the external

sorbent surface. In this part, the instantaneous adsorption is very fast because of the strong interaction between the oil molecules and the external surface of the chitosan-*g*-citronellal Schiff base compared with the chitosan one which supported by the surface area values of the chitosan-*g*-citronellal Schiff base, 112.09 m^2 g^{-1}, compared with chitosan; 57.78 m^2 g^{-1} [21]. After boundary-layer diffusion, the oil entered into the pores of the solid interior sorbent by intraparticle diffusion, as reflected by the second linear part of the plot. This stage describes the gradual adsorption region, where intraparticle diffusion is rate limited. The deviation of straight lines from the origin indicates that intraparticle transport is not the rate-limiting step [43–45]. As seen from this figure, the intraparticle diffusion rate equation fits well to the initial stages of the heavy oil adsorption process for the tested adsorbents; chitosan and chitosan-*g*-citronellal Schiff base.

Table 3 show the calculated values of k_p for chitosan-*g*-citronellal Schiff base is higher than k_p for chitosan due to oil diffusion inside the adsorbent particle in case of chitosan-*g*-citronellal Schiff base is higher than in case of chitosan following the higher pore radius of CH-CIT5 Schiff base, 3.50 nm, compared with 2.2 nm of CH-CIT0; Fig. 1I.

3.7.2. Effect of oil amount and adsorption isotherms

The effect of oil amount variation from 0.5 to 2.5 g was studied to explore the maximum potentials of the developed chitosan-*g*-citronellal matrix (Fig. 3A). A direct relation between the oil amount and the adsorption capacity has been noticed for chitosan and chitosan-*g*-citronellal matrices. The adsorption capacity of the chitosan-*g*-citronellal adsorbent is higher than two folds of the chitosan adsorption capacity. Generally, a concentration gradient between the oil-water liquid and the solid adsorbent phase creates a driving force necessary to overcome all oil resistances between the aqueous and solid phases. Moreover, more oil molecules are available to the adsorbent sites, which enhance the sorption capacity [46].

The adsorption isotherm indicates how the adsorbate molecules distribute between the liquid and solid phases at equilibrium. Therefore, the analysis of the isotherm data by fitting them to different isotherm models is a crucial step to find the suitable model that can be used for design purposes. In this research, an adsorption isotherm study was carried out on two well-known isotherms, that is, Langmuir and Freundlich [47,48].

3.7.3. Langmuir and Freundlich isotherm models

The Langmuir model is obtained below the ideal assumption of a homogenous adsorption surface and represented as follows: [44,47,49].

$$\frac{C_e}{q_e} = \frac{1}{q_m K} + \frac{C_e}{q_m} \tag{7}$$

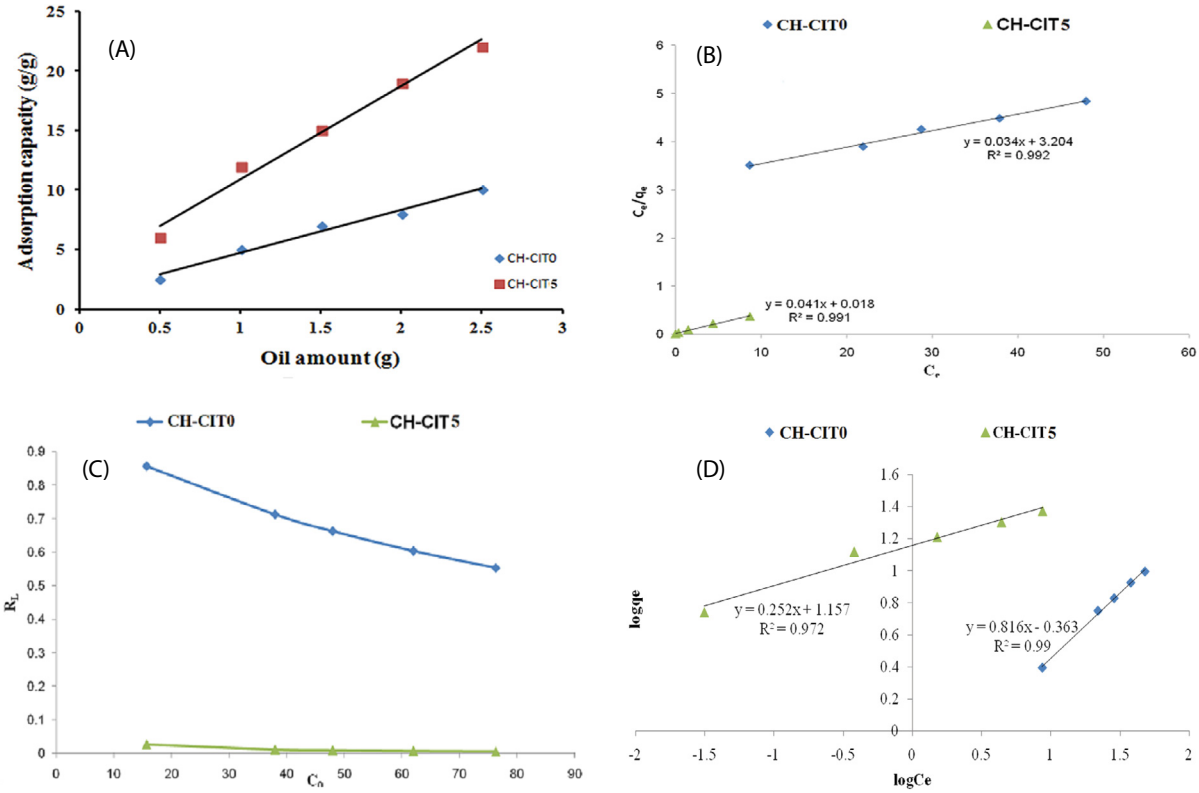

Fig. 3. (A) Effect of oil amount on adsorption capacity of chitosan and chitosan-*g*-citronellal Schiff base. (B) Langmuir plot of heavy crude oil adsorption by (a) chitosan and (b) chitosan-*g*-citronellal Schiff base at 25°C. (C) Dimensionless constant separation factor for chitosan and chitosan-*g*-citronellal Schiff base in case of heavy crude oil adsorption. (D) Freundlich plot of heavy oil adsorption by chitosan and chitosan-*g*-citronellal Schiff base at 25°C.

where q_e is the metal uptake at equilibrium (g g^{-1}); q_{max} is the maximum Langmuir uptake (g g^{-1}); C_e is the final metal concentration at equilibrium (g L^{-1}); b is the Langmuir affinity constant (L g^{-1}).

Fig. 3B shows the Langmuir plots of heavy crude oil at 25°C by chitosan and chitosan-*g*-citronellal Schiff base [50]. The Langmuir isotherm constants q_m and b were calculated from the particular slope and intercept of the linear plot of C_e/q_e against C_e, and the values are presented in Table 4.

The essential features of the Langmuir isotherm can be expressed in terms of a dimensionless constant separation factor (R_L), which is defined as [40].

$$R_L = \frac{1}{1 + KC_0} \tag{8}$$

where K is the Langmuir constant and C_0 is the initial metal concentration (g L^{-1}), and the value of R_L indicates the type of isotherm to be either unfavorable ($R_L > 1$), linear ($R_L = 1$), favorable ($0 < R_L < 1$) or irreversible ($R_L = 0$) [44]. The calculated R_L values at different amounts of heavy crude oil for chitosan and chitosan-*g*-citronellal Schiff base are shown in Fig. 3C. It can be seen that the R_L value drops into the range 0–1 in all experimental systems, which confirms the good uptake of the heavy oil process. Lower R_L values at a higher amount of oil showed that adsorption was more favourable at a higher amount of oil.

The empirical Freundlich isotherm, based on sorption on the heterogeneous surface, can be derived assuming a logarithmic decrease in the enthalpy of sorption with the increase in the fraction of occupied sites and is given by: [47,51].

$$\ln q_e = \ln K_F + \frac{1}{n_f} \ln C_e \tag{9}$$

where K_F and $1/n$ are the Freundlich constants characteristics of the system, indicating the sorption capacity and sorption intensity, and the Freundlich constants can be determined from their intercept and slope.

Fig. 3D shows the Freundlich plots of heavy crude oil at the same temperatures by chitosan and chitosan-*g*-citronellal Schiff [44]. The Freundlich isotherm constants K_F and $1/n$ values are presented in Table 4. From the table it is clear that the values of $1/n$ are less than 1 represents favourable adsorption [52,53]. The correlation coefficient R^2 values indicate an excellent mathematical fit of the heavy crude oil adsorption process to both Langmuir and Freundlich models. The obtained results follow our previously published one concerning the kinetic and thermodynamic studies for the sorptive removal of crude oil spills using a low-cost chitosan-poly(butyl acrylate) grafted copolymer [22].

3.7.4. Adsorption thermodynamics

The thermodynamic parameters, such as a change in Gibbs free energy ($\Delta G°$), change in enthalpy ($\Delta H°$), and change in entropy ($\Delta S°$) of heavy oil adsorbed by chitosan and chitosan-*g*-citronellal Schiff are calculated by Eqs. (10)–(12): [44,47].

The Gibbs free energy change of the adsorption process is related to the equilibrium constant by the equation:

$$\Delta G° = -RT \ln b \tag{10}$$

where $\Delta G°$ is the standard free energy change (kJ mol^{-1}), T the absolute temperature (K) and R (8.3145 J mol^{-1} K^{-1}) is the ideal gas constant, b (mg g^{-1}) an equilibrium constant obtained Langmuir constant.

According to thermodynamics, the Gibbs free energy change is also related to the entropy change and heat of adsorption at constant temperature by the following equation:

$$\Delta G° = \Delta H° - T\Delta S° \tag{11}$$

$$\ln b = \frac{\Delta S}{R} - \frac{\Delta H}{RT} \tag{12}$$

where $\Delta H°$ is enthalpy change (kJ mol^{-1}), $\Delta S°$ entropy change (kJ mol^{-1} K^{-1}), $\Delta H°$ and $\Delta S°$ can be calculated from the plot of ($\ln b$) vs. ($1/T$).

The values of $\Delta S°$ and $\Delta H°$ are calculated from the slopes and intercepts of the linear plots of $\ln b$ vs. $1/T$ (Fig. 4), $\Delta G°$ is obtained using Eq. (10). The thermodynamic parameters of heavy oil adsorbed by chitosan and chitosan-*g*-citronellal Schiff are listed in Table 5. The positive values of $\Delta H°$ suggest that the interaction of heavy oil adsorbed by chitosan-*g*-citronellal Schiff is endothermic, which is supported by the increased adsorption of heavy crude oil with a rise in temperature [22,54]. The negative value of $\Delta G°$ indicates the spontaneous nature of the adsorption. Additionally, the variance of the ΔG diminishes with escalating temperatures regardless of the nature of adsorbent [22].

The positive entropy $\Delta S°$ of chitosan and chitosan-*g*-citronellal Schiff base indicate that process was caused by the decrease in the degree of freedom of the adsorbed species and this positive value of heavy crude oil suggested

Table 4
Isotherm parameters for heavy crude oil adsorption onto chitosan and chitosan-*g*-citronellal Schiff base

Langmuir isotherm						Freundlich isotherm					
Chitosan			Chitosan-*g*-citronellal Schiff base			Chitosan			Chitosan-*g*-citronellal Schiff base		
b	q_{max}	R^2	b	q_{max}	R^2	K_F	$1/n$	R^2	K_F	$1/n$	R^2
0.011	29.4	0.992	2.28	24.4	0.991	0.43	0.81	0.99	18.88	0.09	0.977

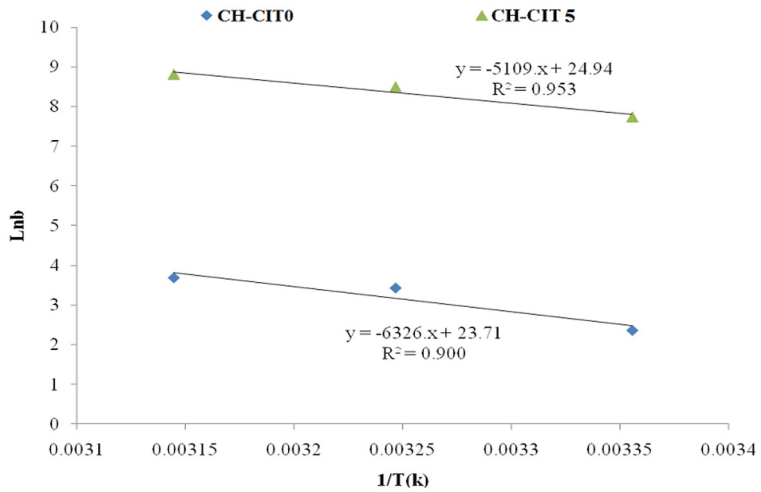

Fig. 4. Van't Hoff plot of heavy crude oil adsorption by chitosan and chitosan-*g*-citronellal Schiff base.

Table 5
Thermodynamics parameter for the adsorption of heavy oil onto chitosan and chitosan-*g*-citronellal Schiff base

T (°C)	ln*b*	Δ*G* (kJ mol^{-1})	Δ*S* (kJ mol^{-1} K^{-1})	Δ*H* (kJ mol^{-1})	R^2
Chitosan					
25	2.36	–7.99	0.197	52.59	0.900
35	3.43	–8.79			
45	3.69	–9.61			
Chitosan-*g*-citronellal Schiff base					
25	7.73	–20.19	0.207	42.48	0.953
35	8.49	–21.46			
45	8.81	–21.73			

that the randomness increased at the solid–liquid interface during the adsorption of heavy oil on chitosan and chitosan-*g*-citronellal Schiff base [22,51].

3.8. Regeneration study

The reusability of the dveloped adsorbent is a cricual issue in evaluation of the cost effective matter. The samples CH-CIT0 and CH-CIT5 Schiff base have been reused for successive seven adsorption–desorption cycles of heavy crude oils. The adsorption capacity and the oil spill removal (%) of both adsorbents have been estimated and tabulated in Table 6. From the table it is clear that the adsorption capacity of the unmodified chitosan (CH-CIT0) has lost 50% of its adsorption capacity estimated at cycle 1 after the seventh cycle. On the other hand, the chitosan-*g*-citronellal Schiff base (CH-CIT5) kept 77% of its adsorption capacity. The CH-CIT5 kept 377% of the CH-CIT0 after the seventh cycle. This finding is emphasis the success of the chitosan-*g*-citronellal Schiff base (CH-CIT5) in the oil spills removal. Both adsorbents show decline of the adsorption capacity with successive adsorption–desorption cycles. The decline behavior of the CH-CIT0 adsorbent is higher than the chitosan-*g*-citronellal Schiff base (CH-CIT5). The decline behavior of the adsorption behavior is accordance with other published results by other authors [55–60]. That behavior could be explained according to the S_{BET} of CH-CIT0, and CH-CIT5 Schiff base; 57.78 and 112.09 m^2 g^{-1}, and the pore radius of CH-CIT0, and CH-CIT5 Schiff base were 2.2 and 3.50 nm. The higher surface area and pore radius of the CH-CIT5 Schiff base facilitates the removal of the adsorbed oil spills more than the CH-CIT0. Mishra and Balasubramanian [55] developed nanostructured camphor soot (CS) particles and PVDF–camphor soot composite for emphatic oil–water separation. They found that after the completion of the first cycle, that is, elimination of oil, is accompanied by an abrupt change in the porous nanotube structure and packing of CS particles, consequently decreasing the absorption capacity. However, after the second cycle there is a trifling change in the structure, so the absorption capacity remains constant henceforth [55]. Li et al. [56] developed a self-established needleless melt-electrospinning process was used to produce PLA ultrafine fibers with diameters in the range of 800 nm^{-9} um. The prepared PLA ultrafine fibers exhibited super-hydrophobicity making it a potential candidate in marine oil spill recovery. The oil sorption capability of these fibers is as high as 118 g g^{-1} for crude oil. Even after seven cycles of reuse, the fiber still maintained about 60% of its initial capacity of sorption. The sudden decrease of oil sorption capacity from the first to the second cycle is mainly attributed to the irreversible deformation or general deterioration of the fiber assembly due to strong mechanical pressure and residual oils trapped in the void of fibrous sorbent.

Elias et al. [57] investigated the curaua fibers and their effect on the oil absorption capability of the cardanol–furfural resin. They found that after the oil removal tests, gravimetric experiments have shown that 90% of the sorbent was recovered from the oil using a filtering process. The recovered material could be reused in further clean-up experiments where in the first, second, and third reuse cycles, removed 12.65, 11.25, and 10.80 g g^{-1} of oil from the

Table 6
Oil adsorption capacity of chitosan and chitosan-*g*-citronellal derivative with successive adsorption cycles

Sample code	Cycle 1	Cycle 2	Cycle 3	Cycle 4	Cycle 5	Cycle 6	Cycle 7
Oil adsorption capacity (g g^{-1})							
CH-CIT0	9.0	8.5	8.0	7.0	5.7	5.0	4.5
CH-CIT5	22.0	22.0	20.0	19.5	18.0	17.0	17.0
Oil removal efficiency (%)							
CH-CIT0	100	94.44	88.88	77.77	63.33	55.55	50.00
CH-CIT5	100	100	90.91	88.64	81.82	77.27	77.27

water, respectively. Nikkhah et al. [58] modified polyurethane foam structure by integrating cloisite 20A nanoclay into it to enhance the removal of oil contaminants from water. The experimental results showed that the recovery of nanocomposites through washing with petroleum solvent reduces oil removal efficiency. This is due to the lower oil adsorption as a result of structural strength weakening after being washed with toluene. Atta et al. [59] a facile, green, one-step method was suggested to produce monodisperse hydrophobic magnetite nanoparticles capped with 1-allyl-3-imidazoliumoleate at room temperature. The application of the synthesized magnetic nanomaterials for collecting heavy petroleum crude oil from polluted water surfaces was a goal of their work. The obtained data showed that the magnetite was reused for 5 cycles after separation with an external magnet from crude oil diluted with diesel fuel. The removal efficiency reduced by 4%–10%, depend on the operational conditions. Chen et al. [60], synthesis highly hydrophobic floating magnetic polymer nanocomposites for the removal of oils from water surface. The nanocomposites also had an excellent recyclability in the oil-absorbent capacity. Only slight linear decrement changes in water contact angles from 153° were observed in the first adsorption cycle to 140° at the six cycle of the study.

4. Conclusion

The present work evaluated the kinetic, isothermal, and thermodynamic of heavy crude oil spills adsorption by novel chitosan-*g*-citronellal Schiff base. The developed chitosan and novel chitosan-*g*-citronellal Schiff base adsorbents were characterized under advanced analytical tools such as FTIR, ^{1}H NMR spectroscopy, thermal analysis (TGA) and SEM analysis.

The adsorption process followed the pseudo-second-order model, and the equilibrium data were sufficiently fitted with both Langmuir and Freundlich isotherm models. The Langmuir maximum monolayer adsorption capacity for heavy crude oil adsorption was found 29.4 (g g^{-1}) and 24.40 g g^{-1} for the chitosan and the chitosan-*g*-citronellal Schiff base adsorbents. Thermodynamic parameters computed from Van't Hoff plot confirmed the process to be exothermic, favourable and spontaneous. The experimental results revealed a significant increase in the oil adsorption capacity of chitosan-*g*-citronellal Schiff base 22 g g^{-1} compared to the chitosan 9 g g^{-1} within the studied conditions increasing its hydrophobic character after Schiff base formation. The obtained result is higher than other published results by the study of Kumar et al. [61] where developed superparamagnetic iron-oxide nanoparticles (SPION) nanocomposite with b-cyclodextrin (SPION/b-CD) has an oil retention capacity of 7.2 g g^{-1}.

Moreover, the BET analysis of the developed chitosan-*g*-citronellal Schiff base exhibited a higher surface area, 112.09 m^2 g^{-1}, compared to neat chitosan; 57.78 m^2 g^{-1}. Furthermore, the Barrett–Joyner–Halenda pore size distributions revealed that the developed chitosan-*g*-citronellal Schiff base exhibited the pore radius of the developed chitosan-*g*-citronellal Schiff base is 3.50 nm, compared to the chitosan; 2.2 nm. Furthermore, the recyclability of the developed chitosan-*g*-citronellal Schiff base has been proved while kept 77% of its oil adsorption capacity (17 g g^{-1}) after seven cycles compared with 50% of the chitosan counterpart; 4.5 g g^{-1}.

References

[1] T.R. Annunciado, T.H.D. Sydenstricker, S.C. Amico, Experimental investigation of various vegetable fibers as sorbent materials for oil spills, Mar. Pollut. Bull., 50 (2005) 1340–1346.
[2] M. Keshawy, T. Abd El-Moghny, A.-R.M. Abdul-Raheim, K.I. Kabel, S.H. El-Hamouly, Synthesis and characterization of oil sorbent based on hydroxypropyl cellulose acrylate, Egypt. J. Pet., 22 (2013) 539–548.
[3] A. Srinivasan, T. Viraraghavan, Removal of oil by walnut shell media, Bioresour. Technol., 99 (2008) 8217–8210.
[4] S. Aboulhadeed, Development of Polymeric Composite Materials for Oil Spill Removal, M.Sc. Thesis, Alexandria University, Alexandria, Egypt, 2016, pp. 1–150.
[5] A. Raymon, R. Karthik, Reclaiming aged transformer oil with activated bentonite and enhancing reclaimed and fresh transformer oils with antioxidants, IEEE Trans. Dielectr. Electr. Insul., 21 (2015) 548–555.
[6] M.S. Mohy Eldin, Y.A. Ammar, T.M. Tamer, A.M. Omer, A.A. Ali, Development of oleophilic adsorbent based on chitosan-poly(butyl acrylate) graft copolymer for petroleum oil spill removal, Int. J. Adv. Res., 4 (2016) 2095–2111.
[7] H. Bernard, K. Jakobson, Effectiveness of Device for the Control and Clean-up of Oil Spills, SPE Paper 1525-MS, Presented at Offshore Technology Conference, Houston, Texas, 1–3 May 1972.
[8] A.A. Al-Majed, A.R. Adebayo, M. Enamul Hossain, A sustainable approach to controlling oil spills, J. Environ. Manage., 113 (2012) 213–227.
[9] T.F. Jiao, J. Zhou, J.X. Zhou, L.H. Gao, Y.Y. Xing, X.H. Li, Synthesis and characterization of chitosan-based Schiff base compounds with aromatic substituent groups, Iran. Polym. J., 20 (2011) 123–136.

[10] M.O. Adebajo, R.L. Frost, J.T. Kloprogge, O. Carmody, S. Kokot, Porous materials for oil spill cleanup: a review of synthesis and absorbing properties, J. Porous Mater., 10 (2003) 159–170.
[11] G. Alaa El-Din, A.A. Amer, G. Malsh, M. Hussein, Study on the use of banana peels for oil spill removal, Alexandria Eng. J., 57 (2018) 2061–2068.
[12] E. Wolok, J. Barafi, N. Joshi, R. Girimonte, S. Chakraborty, Study of bio-materials for removal of the oil spill, Arabian J. Geosci., 13 (2020) 1244, doi: 10.1007/s12517-020-06244-3.
[13] A.T. Hoang, S. Nižetić, X.Q. Duong, L. Rowinski, X.P. Nguyen, Advanced super-hydrophobic polymer-based porous absorbents for the treatment of oil-polluted water, Chemosphere, 277 (2021) 130274, doi: 10.1016/j.chemosphere.2021.130274.
[14] R.A.A. Muzzarelli, C. Jeunieux, G.W. Gooday, Chitin in Nature and Technology, Plenum, New York, 1985.
[15] G.K. Moore, G.A.F. Roberts, Reactions of chitosan: preparation and reactivity of Schiff's base derivatives of chitosan, Int. J. Biol. Macromol., 3 (1981) 337–341.
[16] A.M. Omer, B.Y. Eweida, T.M. Tamer, H.M.A. Soliman, S.M. Ali, A.A. Zaatot, M.S. Mohy-Eldin, Removal of oil spills by novel developed amphiphilic chitosan-*g*-citronellal Schiff base polymer, Sci. Rep., 11 (2021) 19879, doi: 10.1038/s41598-021-99241-9.
[17] M.S. Mohy Eldin, Y.A. Ammar, T.M. Tamer, A.M. Omer, A.A. Ali, Development of low-cost chitosan derivatives based on marine waste sources as oil adsorptive materials: I. preparation and characterization, Desal. Water Treat., 72 (2017) 41–51.
[18] M.S. Mohy Eldin, Y.A. Ammar, T.M. Tamer, A.M. Omer, A.A. Ali, Development of oleophilic adsorbent based on chitosan-poly(butyl acrylate) graft copolymer for petroleum oil spill removal, Int. J. Adv. Res., 4 (2016) 2095–2111.
[19] M.S. Mohy Eldin, Y.A. Ammar, T.M. Tamer, A.M. Omer, A.A. Ali, Development of a low-cost oleophilic adsorbent based on aminated chitosan-poly(butyl acrylate) graft copolymer for marine oil spill cleanup, Int. J. Adv. Res., 4 (2016) 2080–2094.
[20] A.M. Omer, R.E. Khalifa, T.M. Tamer, M. Elnouby, A.M. Hamed, Y.A. Ammar, A.A. Ali, M. Gouda, M.S. Mohy Eldin, Fabrication of a novel low-cost superoleophilic nonanyl chitosan-poly(butyl acrylate) grafted copolymer for the adsorptive removal of crude oil spills, Int. J. Biol. Macromol., 140 (2019) 588–599.
[21] R.E. Khalifa, A.M. Omer, T.M. Tamer, A.A. Ali, Y.A. Ammar, M.S. Mohy Eldin, Efficient eco-friendly crude oil adsorptive chitosan derivatives: kinetics, equilibrium and thermodynamic studies, Desal. Water. Treat., 159 (2019) 269–281.
[22] A.M. Omer, R.E. Khalifa, T.M. Tamer, A.A. Ali, Y.A. Ammar, M.S. Mohy Eldin, Kinetic and thermodynamic studies for the sorptive removal of crude oil spills using a low-cost chitosan-poly(butyl acrylate) grafted copolymer, Desal. Water. Treat., 192 (2020) 213–225.
[23] T.M. Tamer, A.M. Omer, R.E. Khalifa, A.A. Ali, Y.A. Ammar, M.S. Mohy Eldin, Aminated chitosan-g-poly(butyl acrylate) copolymer for heavy oil spills removal: kinetic, isotherm, and thermodynamic investigations, Desal. Water Treat., 226 (2021) 319–327.
[24] M.S. Mohy Eldin, A.M. Omer, A.I. Hashem, T.M. Tamer, Preparation, characterization and antimicrobial evaluation of novel cinnamyl chitosan Schiff base, Int. J. Adv. Res., 3 (2015) 741–755.
[25] S. Sashikala, S. Syed Shafi, Synthesis and characterization of chitosan Schiff base derivatives, Der Pharmacia Lettre, 6 (2014) 90–97.
[26] E.-R. Kenawy, F. Imam Abdel-Hay, M.S. Mohy Eldin, T.M. Tamer, E.M. Abo-Elghit Ibrahim, Novel aminated chitosan-aromatic aldehydes Schiff bases: synthesis, characterization and bio-evaluation, Int. J. Adv. Res., 3 (2015) 563–572.
[27] J. Zawadzki, H. Kaczmarek, Thermal treatment of chitosan in various conditions, Carbohydr. Polym., 80 (2010) 394–400.
[28] A. Bazargan, J. Tan, G. McKay, Standardization of oil sorbent performance testing, J. Test. Eval., 43 (2015) 2014–217.
[29] J. Zhang, Q. Wang, A. Wang, Synthesis and characterization of chitosan-g-poly(acrylic acid)/attapulgite superabsorbent composites, Carbohydr. Polym., 68 (2007) 367–374.
[30] G.A. Mun, Z.S. Nurkeeva, S.A. Dergunov, I.K. Nam, T.P. Maimakov, E.M. Shaikhutdinov, S.C. Lee, K. Park, Studies on graft copolymerization of 2-hydroxyethyl acrylate onto chitosan, React. Funct. Polym., 68 (2008) 389–395.
[31] M.R. Kasaai, Determination of the degree of *N*-acetylation for chitin and chitosan by various NMR spectroscopy techniques: a review, Carbohydr. Polym., 79 (2010) 801–810.
[32] A. Hirai, H. Odani, A. Nakajima, Determination of degree of deacetylation of chitosan by ^{1}H NMR spectroscopy, Polym. Bull., 26 (1991) 87–94.
[33] E.A. Soliman, S.M. El-Kousy, H.M. Abd-Elbary, A.R. Abou-zeid, Low molecular weight chitosan-based Schiff bases: synthesis, characterization and antibacterial activity, Am. J. Food Technol., 8 (2013) 17–30.
[34] M. Lavertu, Z. Xia, A.N. Serreqi, M. Berrada, A. Rodrigues, D. Wang, M.D. Buschmann, A. Gupta, A validated ^{1}H NMR method for the determination of the degree of deacetylation of chitosan, J. Pharm. Biomed. Anal., 32 (2003) 1149–1158.
[35] A. Pawlak, M. Mucha, Thermogravimetric and FTIR studies of chitosan blends, Thermochim. Acta, 396 (2003) 153–166.
[36] L. Zhang, P. Hu, J. Wang, Q. Liu, R. Huang, Adsorption of methyl orange (MO) by Zr(IV)-immobilized cross-linked chitosan/bentonite composite, Int. J. Biol. Macromol., 81 (2015) 818–827.
[37] M. Chen, W. Jiang, F. Wang, P. Shen, P. Ma, J. Gu, F. Li, Synthesis of highly hydrophobic floating magnetic polymer nanocomposites for the removal of oils from water surface, Appl. Surf. Sci., 286 (2013) 249–256.
[38] W. Jintao, Zh. Yian, W. Aiqin, Kinetic and thermodynamic studies on the removal of oil from water using superhydrophobic kapok fiber, Water Environ. Res., 86 (2014) 360–365.
[39] W. Jintao, Zh. Yian, W. Aiqin, Coated kapok fiber for removal of spilled oil, Mar. Pollut. Bull., 69 (2013) 91–96.
[40] M.F. Elkady, H. Mohamed, A. Reham, Equilibrium and kinetics behavior of oil spill process onto synthesized nano-activated carbon, Am. J. Appl. Chem., 3 (2015) 22–30.
[41] L. Setti, S. Mazzieri, P.G. Pifferi, Enhanced degradation of heavy oil in an aqueous system by a *Pseudomonas* sp. in the presence of natural and synthetic sorbents, Bioresour. Technol., 67 (1999) 191–199.
[42] F.C.F. Barros, L. Vasconcellos, C. Grombone, T.V. Carvalho, R.F.D. Nascimento, Removal of petroleum spill in water by chitin and chitosan, Orbital – The Electron. J. Chem., 6 (2014) 70–74.
[43] A. Bazargan, J. Tan, G. McKay, Standardization of oil sorbent performance testing, J. Test. Eval., 43 (2015) 1–10.
[44] S.S.D. Elanchezhiyan, N. Sivasurian, S. Meenakshi, Recovery of oil from oil-in-water emulsion using biopolymers by adsorptive method, Int. J. Biol. Macromol., 70 (2014) 399–407.
[45] J.O. Nwadiogbu, V.I.E. Ajiwe, P.A.C. Okoye, Removal of crude oil from aqueous medium by sorption on hydrophobic corncobs: equilibrium and kinetic studies, J. Taibah Univ. Sci., 10 (2015) 56–63.
[46] O. Khaled, E. Mona, Y.E. Mohamed, Treatment of oil–water emulsions by adsorption onto activated carbon, bentonite and deposited carbon, Egypt. J. Pet., 20 (2011) 9–15.
[47] A.E.E. Noha, M.A. Safa, A.F. Hassan, H.K. Abdelaziz, E. Mohamed, A.H. Hesham, Green synthesis of graphene from recycled PET bottle wastes for use in the adsorption of dyes in aqueous solution, Ecotoxicol. Environ. Saf., 145 (2017) 57–68.
[48] Z. Aslam, I.A. Hussein, R.A. Shawabkeh, M.A. Parvez, W. Ahmad, Ihsanullah, Adsorption kinetics and modeling of H_2S by treated waste oil fly ash, J. Air Waste Manage. Assoc., 69 (2019) 246–257.
[49] Y. Nacèra, B. Aicha, Equilibrium and kinetic modelling of methylene blue biosorption by pretreated dead *Streptomyces rimosus*: effect of temperature, Chem. Eng. J., 119 (2006) 121–125.
[50] H.T.T. Duong, R.P. Burford, Effect of foam density, oil viscosity, and temperature on oil sorption behavior of polyurethane, J. Appl. Polym. Sci., 99 (2005) 360–367.
[51] P. Min, L. Xumeng, X. Jingjing, H. Xiaoming, Kinetic, equilibrium and thermodynamic studies for phosphate adsorption on

aluminum hydroxide modified palygorskite nano-composites, RSC Adv., 7 (2017) 4492–4500.
[52] R. Asadpour, N. Bin Sapari, Z.Z. Tuan, H. Jusoh, A. Riahi, O.K. Uka, Application of sorbent materials in oil spill management: a review, Caspian J. Appl. Sci. Res., 2 (2013) 46–58.
[53] M.S. Mohy Eldin, K.A. Alamry, Z.A. Khan, A.E.M. Mekky, T.S. Saleh, Kinetic and equilibrium studies of chromium(VI) metal ions adsorption using Amberlite IRA-420 anions exchanger, Desal. Water Treat., 62 (2017) 377–386.
[54] Y. Sayiter, Kinetic and isotherm analysis of Cu(II) adsorption onto almond shell (*Prunus dulcis*), Ecol. Chem. Eng. S, 24 (2017) 87–106.
[55] P. Mishra, K. Balasubramanian, Nanostructured microporous polymer composite imprinted with superhydrophobic camphor soot, for emphatic oil–water separation, RSC Adv., 4 (2014) 53291–53296.
[56] H. Li, Y. Li, W. Yang, L. Cheng, J. Tan, Needleless melt-electrospinning of biodegradable poly(lactic acid) ultrafine fibers for the removal of oil from water, Polymers, 9 (2017) 3, doi: 10.3390/polym9020003.
[57] E. Elias, R. Costa, F. Marques, G. Oliveira, Q. Guo, S. Thomas, F.G. Souza Jr., Oil-spill cleanup: the influence of acetylated curaua fibers on the oil-removal capability of magnetic composites, J. Appl. Polym. Sci., 132 (2015) 41732, doi: 10.1002/app.41732.
[58] A.A. Nikkhah, H. Zilouei, A. Asadinezhad, A. Keshavarz, Removal of oil from water using polyurethane foam modified with nanoclay, Chem. Eng. J., 262 (2015) 278–285.
[59] A.M. Atta, A.O. Ezzat, A.I. Hashem, Synthesis and application of monodisperse hydrophobic magnetite nanoparticles as an oil spill collector using an ionic liquid, RSC Adv., 7 (2017) 16524–16530.
[60] M. Chen, W. Jiang, F. Wang, P. Shen, P. Ma, J. Gu, J. Mao, F. Li, Synthesis of highly hydrophobic floating magnetic polymer nanocomposites for the removal of oils from water surface, Appl. Surf. Sci., 286 (2013) 249–256.
[61] A. Kumar, G. Sharma, Mu. Naushad, S. Thakur, SPION/β-cyclodextrin core–shell nanostructures for oil spill remediation and organic pollutant removal from waste water, Chem. Eng. J., 280 (2015) 175–187.